


 Cite this: *RSC Adv.*, 2022, 12, 14639


Received 5th April 2022

Accepted 6th May 2022

DOI: 10.1039/d2ra02202h

[rsc.li/rsc-advances](https://rsc.li/rsc-advances)

## Preparation and characterization of an edible metal–organic framework/rice wine residue composite†

 Teer Ba, Chenyang Shen, Xiaoshan Zhang and Chang-jun Liu \*

In this communication, using rice wine residue (RWR) as the support, an edible  $\gamma$ -cyclodextrin-metal–organic framework/RWR ( $\gamma$ -CD-MOF/RWR) composite with a macroscopic morphology was synthesized. The obtained edible composite is promising for applications in drug delivery, adsorption, food processing, and others.

As a typical class of porous materials, metal–organic frameworks (MOFs) have attracted increasing attention since being first proposed by Yaghi and co-workers.<sup>1</sup> Over the past two decades, owing to their large surface area, ultrahigh porosity and tunable pore size,<sup>2</sup> MOFs have exhibited great prospects for gas storage and separation,<sup>3,4</sup> catalysis,<sup>5–8</sup> sensors,<sup>9</sup> drug delivery,<sup>10–12</sup> *etc.* Among numerous reported MOFs,  $\gamma$ -cyclodextrin-MOF ( $\gamma$ -CD-MOF), which is connected by the ( $\gamma$ -CD)<sub>6</sub> units of alkaline earth metal ions, was initially synthesized and reported by Stoddart *et al.*<sup>13,14</sup> in the 2010s. Owing to the –OCCO– groups derived from  $\gamma$ -CD, this kind of MOF is edible and therefore opens a new path for preparing green, biocompatible and edible MOF materials.<sup>13,15,16</sup> For example, Stoddart *et al.*<sup>11</sup> reported a co-crystallization approach to trap ibuprofen and lansoprazole inside  $\gamma$ -CD-MOF, and the resultant composite microspheres can be used for sustained drug delivery. Zhang *et al.*<sup>17</sup> proposed a strategy to graft cholesterol over the surface of  $\gamma$ -CD-MOF to form a protective hydrophobic layer to improve its water stability. Many researchers succeeded in preparing oral delivery medicine with high drug loading and an enhanced therapeutic effect by combining the drug molecules with  $\gamma$ -CD-MOF.<sup>16,18–20</sup> These works present the excellent application prospects of  $\gamma$ -CD-MOF in the medical field.

Since MOFs possess so many attractive advantages, extensive studies have focused on combining MOFs with many other functional materials (metal nanoparticles, quantum dots, carbon matrices and polyoxometalates, *etc.*) by means of the synergistic effect, leading to the formation of novel composites designed for targeted applications.<sup>21–28</sup> However, these reported composites were still presented as loose powders, which may not be convenient for the applications. Therefore, the question

of how to prepare MOFs-based composites for larger particles at low cost is of great significance. On the other hand, as a traditional alcoholic beverage, rice wine has been popular in southern China and some other Asian nations for thousands of years.<sup>29</sup> The rice wine lees or rice wine residue (RWR) is a by-product of the fermentation process of rice wine. It is a mixture of proteins, amino acids and polysaccharides. It is traditionally a health food in some Asian nations.<sup>30</sup> The edibility, extensive source, low cost and specific macroscopic shape make RWR a potential functional material for further use of MOFs.

Herein, a facile and environmental-friendly strategy has been developed to realize the growth of  $\gamma$ -CD-MOF on rice wine residue, resulting in the formation of an edible MOF/RWR composite in the shape of rice grains. The material characterization confirmed the obtained composite possesses the characteristics of MOF. Except for the edible  $\gamma$ -CD-MOF/RWR, other MOF/RWR composites (HKUST-1, ZIF-67 and MIL-100(Fe)/RWR composites; shown in Fig. S1†) were prepared to demonstrate the universality of this synthesis strategy.

The synthesis procedure of the  $\gamma$ -CD-MOF/RWR composite is schematically illustrated in Fig. 1. The rice wine residue was soaked in deionized water for 12 h and then washed with deionized water three times before vacuum freeze-drying. Similar to the synthesis of  $\gamma$ -CD-MOF powder,<sup>15</sup> KOH was dissolved into water. Then certain amounts of the aforementioned dry rice wine residue were soaked into the K<sup>+</sup>-containing solution for 2 h in order to absorb the sufficient potassium ions. K<sup>+</sup> was then linked by the coordination of –OCCO– units in  $\gamma$ -CD and RWR with the three-dimensional interconnected network. After vapor diffusion of MeOH and some other procedures described in the synthesis of  $\gamma$ -CD-MOF powder (seen in ESI), the  $\gamma$ -CD-MOF/RWR composite (Fig. 2) was obtained. This method is convenient as no extra binders are needed during the whole process. The same procedure was employed to prepare the RWR composites with other MOFs (HKUST-1, ZIF-67 and

Collaborative Innovation Center of Chemical Science & Engineering, School of Chemical Engineering and Technology, Tianjin University, Tianjin 300072, China.  
 E-mail: [cjl@tju.edu.cn](mailto:cjl@tju.edu.cn)

† Electronic supplementary information (ESI) available. See <https://doi.org/10.1039/d2ra02202h>



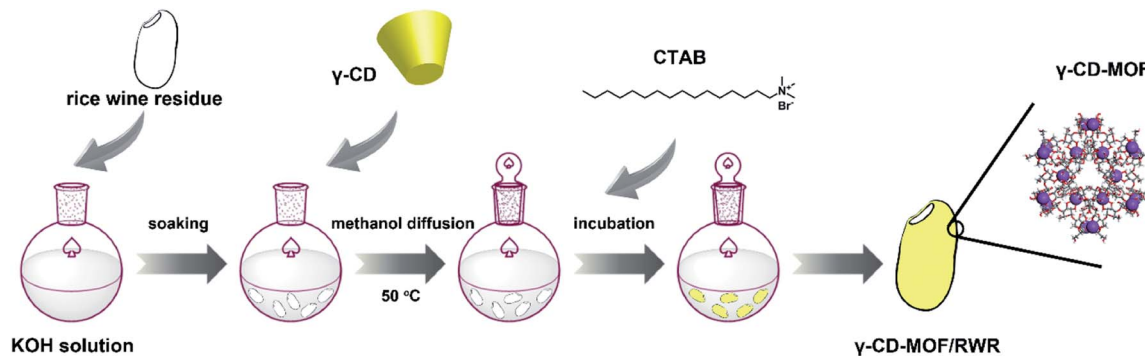


Fig. 1 Schematic illustration of the synthesis procedure of  $\gamma$ -CD-MOF/RWR composite.



Fig. 2 Digital photo of the  $\gamma$ -CD-MOF/RWR composite.

MIL-100(Fe)). And the syntheses are briefly described in the ESI. The images of the obtained composites are shown in Fig. S1.†

The rice wine residue, of which the elemental analysis is shown in Table S1,† is mainly composed of polysaccharides and proteins. Thus, a broad peak at around  $22.2^\circ$  in the XRD patterns of rice wine residue can be observed (Fig. S2)†, which is due to its poor crystallinity.<sup>31</sup> The XRD patterns of  $\gamma$ -CD-MOF and  $\gamma$ -CD-MOF/RWR composite samples are shown in Fig. 3a. The characteristic peaks at  $5.6^\circ$ ,  $6.9^\circ$ ,  $13.3^\circ$ ,  $16.6^\circ$ ,  $20.6^\circ$  and  $23.2^\circ$ , observed from the XRD patterns of  $\gamma$ -CD-MOF, agree with the previously reported works.<sup>32,33</sup> Meanwhile, compared with  $\gamma$ -CD-MOF, the  $\gamma$ -CD-MOF/RWR composite shows similar characteristic peaks with lower intensity, indicating a lower crystallinity of the MOF within the composite. Fig. 3b shows the FT-IR spectra of different samples. Compared with the rice wine residue, the peaks in regions 1 and 2 of  $\gamma$ -CD-MOF and  $\gamma$ -CD-MOF/RWR can be ascribed to the stretching vibration of  $-\text{CH}_2$

and  $-\text{C}-\text{O}-\text{C}-$  of the MOF, respectively.<sup>15,34</sup> These results further confirm the formation of the  $\gamma$ -CD-MOF in the  $\gamma$ -CD-MOF/RWR composite.

The SEM images were collected to further investigate the micromorphology of the as-prepared samples. As shown in Fig. 4a, a three-dimensional layered network structure and rich macropores of the rice wine residue rough surface can be seen.  $\gamma$ -CD-MOF (Fig. 4b) exhibits a uniform body-centered cubic shape with an average size of  $4.27 \mu\text{m}$ , which is in accordance

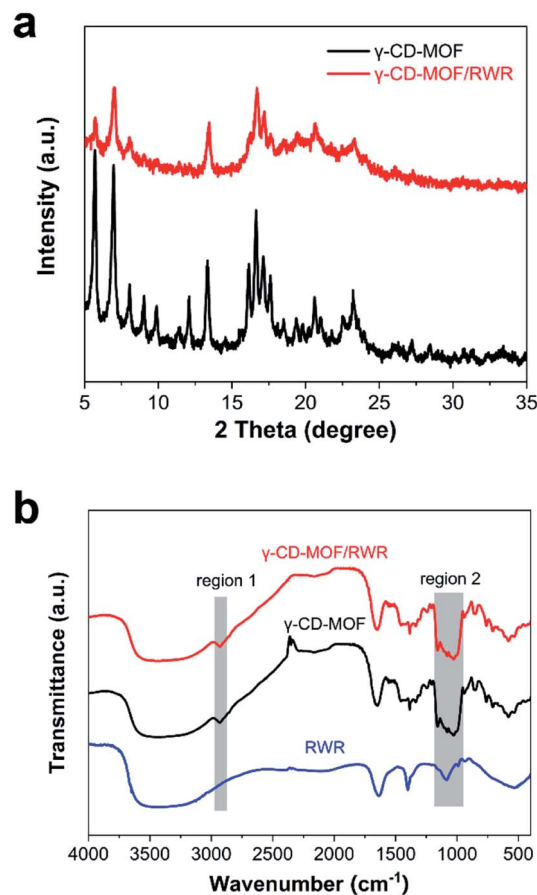


Fig. 3 XRD patterns (a) and FT-IR spectra (b) of  $\gamma$ -CD-MOF/RWR composite,  $\gamma$ -CD-MOF and RWR.



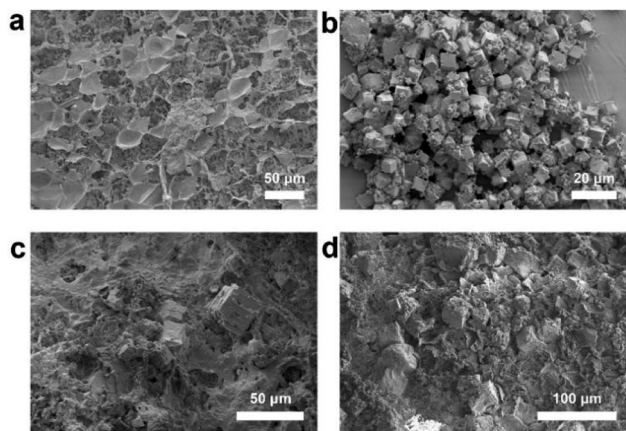


Fig. 4 SEM images of rice wine residue (a),  $\gamma$ -CD-MOF (b) and  $\gamma$ -CD-MOF/RWR composite (c and d).

with the reported works.<sup>15,35,36</sup> Meanwhile, the images of the  $\gamma$ -CD-MOF/RWR composite (Fig. 4c and d) show that the cubic  $\gamma$ -CD-MOF crystals are well dispersed on the surface of the rice wine residue and even partially integrated into the framework of the rice wine residue. Compared with the pristine  $\gamma$ -CD-MOF, some  $\gamma$ -CD-MOF in  $\gamma$ -CD-MOF/RWR is not an intact cubic structure, exhibiting a significantly different morphology. This suggests a synergistic effect between the MOF crystals and the rice wine residue during the growth of MOF crystals, rather than a simple physical mixture of the two materials. The thermal stability of the  $\gamma$ -CD-MOF/RWR composite was investigated *via* TGA analysis. As shown in Fig. S3,† the decomposition temperature of  $\gamma$ -CD-MOF/RWR composite slightly increased compared with those of pristine  $\gamma$ -CD-MOF and rice wine residue. Moreover, the  $\gamma$ -CD-MOF/RWR composite was stable in water, methanol and ethanol (shown in Fig. S4†) even under mild stirring. These results indicate an improved physicochemical stability of  $\gamma$ -CD-MOF after the incorporation of rice wine residue. This finding further confirms the synergistic effect between them.

Fig. 5a shows the nitrogen sorption isotherms of the  $\gamma$ -CD-MOF and  $\gamma$ -CD-MOF/RWR composite. Both pristine  $\gamma$ -CD-MOF and  $\gamma$ -CD-MOF/RWR exhibit typical type-I isotherms, demonstrating their microporous structures. The pore size distributions of pure  $\gamma$ -CD-MOF and  $\gamma$ -CD-MOF/RWR (Fig. 5b) confirm the existence of micropores (between 1 and 2 nm). The calculated Brunauer-Emmett-Teller (BET) surface areas, micropore volume and total pore volume are listed in Table 1. As shown in Table 1, pure  $\gamma$ -CD-MOF possesses a high specific surface area ( $1096 \text{ m}^2 \text{ g}^{-1}$ ), which is consistent with the literature.<sup>35,37</sup> The specific surface area of the  $\gamma$ -CD-MOF/RWR composite is  $651 \text{ m}^2 \text{ g}^{-1}$ , which is significantly higher than that of the pure rice wine residue ( $10.8 \text{ m}^2 \text{ g}^{-1}$ ). Thus, the increase in the specific surface area of  $\gamma$ -CD-MOF/RWR composite can be attributed to the growth of  $\gamma$ -CD-MOF on the RWR support. Therefore,  $\gamma$ -CD-MOF/RWR composite inherits both the high porosity of  $\gamma$ -CD-MOF and the macroscopic morphology of rice wine residue, which should contribute to its practical applications.

To further investigate the universality of this synthesis strategy, different MOFs (*i.e.*, HKUST-1, ZIF-67 and MIL-100(Fe)) and their corresponding composites were prepared and investigated. Digital photos of different samples (Fig. S1†) show that all composites maintain the original shape of rice wine residue. Meanwhile, the colours of composites vary with different MOFs. Moreover, the XRD results in Fig. S5–S7† confirm the growth of various MOFs on rice wine residue. Therefore, these results demonstrate that this synthesis strategy is universally applicable. Moreover, compared to other MOF-based composites, it should be noted that the composites synthesized *via* this strategy exhibit a macroscopic shape rather than being a loosely packed fine powder. Considering the industrial demand for enhanced mass transfer with low pressure drop, the MOF/RWR composites are promising for industrial applications.

In conclusion, a facile and environmental-friendly method has been developed to prepare a  $\gamma$ -CD-MOF/RWR composite without extra binders. The edibility of  $\gamma$ -CD-MOF and rice wine residue has been well demonstrated in the literature,<sup>16,38–42</sup> demonstrating that the  $\gamma$ -CD-MOF/RWR composite is also

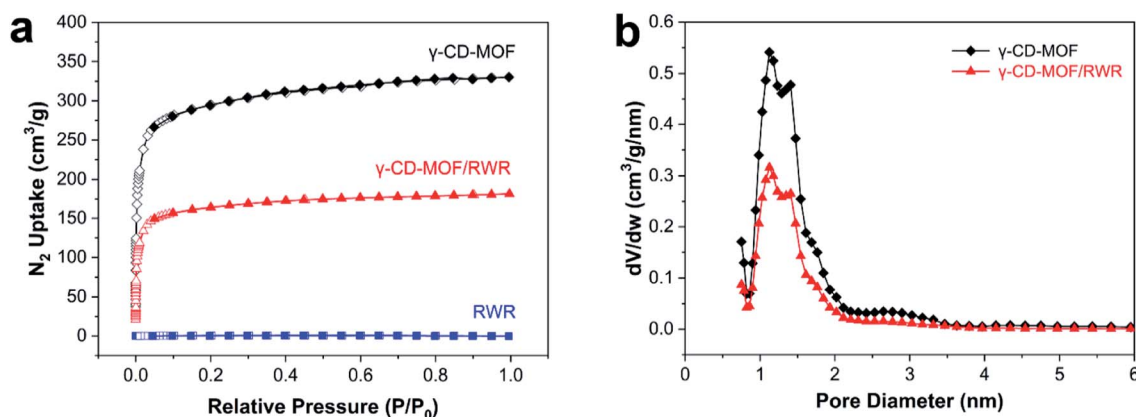


Fig. 5  $\text{N}_2$  adsorption and desorption isotherms (a) and pore size distributions (b) of  $\gamma$ -CD-MOF/RWR composite and corresponding comparative samples.

**Table 1** Summary of the BET areas ( $S_{\text{BET}}$ ), micropore volume ( $V_{\text{micro}}$ ) and total pore volume ( $V_{\text{tot}}$ ) of  $\gamma$ -CD-MOF,  $\gamma$ -CD-MOF/RWR composite and pure rice wine residue

Samples	$S_{\text{BET}}$ ( $\text{m}^2 \text{g}^{-1}$ )	$V_{\text{micro}}$ ( $\text{cm}^3 \text{g}^{-1}$ )	$V_{\text{tot}}$ ( $\text{cm}^3 \text{g}^{-1}$ )
$\gamma$ -CD-MOF	1096	0.39	0.51
$\gamma$ -CD-MOF/RWR composite	651	0.22	0.28
RWR	10.8	0.024	0.038

edible. The growth of  $\gamma$ -CD-MOF on rice wine residue is based on the synergetic effect between the two components, rather than a simple physical mixture of two materials. Due to the large pore size and high BET specific surface area, the edible  $\gamma$ -CD-MOF/RWR composite in the shape of rice will be more convenient for applications including drug delivery, food processing, adsorption, gas separation, catalysis and others. The MOF/RWR composites can be also an excellent precursor for carbon-based material or catalysts.<sup>30</sup> The synthetic method developed here might give inspiration for designing and preparing MOF-based composites in the shape of rice with the utilization of RWR.

## Author contributions

Teer Ba: methodology, investigation, visualization, writing – original draft. Chenyang Shen: conceptualization, methodology, formal analysis, investigation, writing – review & editing. Xiaoshan Zhang: conceptualization, methodology and investigation. Chang-jun Liu: resources, investigation, supervision, writing – review & editing.

## Conflicts of interest

There are no conflicts to declare.

## Acknowledgements

This work was supported by the National Natural Science Foundation of China (No. 22138009).

## References

- H. Li, M. Eddaoudi, M. O'Keeffe and O. M. Yaghi, *Nature*, 1999, **402**, 276–279.
- W. Xiang, Y. Zhang, Y. Chen, C.-j. Liu and X. Tu, *J. Mater. Chem. A*, 2020, **8**, 21526–21546.
- J. Lee, Y. Seo, D. W. Kang, S. Park, H. Kim, J. Kim, K. Kim, C. S. Hong, D.-W. Lim and E. Lee, *RSC Adv.*, 2022, **12**, 7605–7611.
- J. Liu, Y. Wei, P. Li, Y. Zhao and R. Zou, *J. Phys. Chem. C*, 2017, **121**, 13249–13255.
- N. Zaman, T. Noor and N. Iqbal, *RSC Adv.*, 2021, **11**, 21904–21925.
- J. Ye and C.-j. Liu, *Chem. Commun.*, 2011, **47**, 2167–2169.
- W. Xiang, Z. Sun, Y. Wu, L.-N. He and C.-j. Liu, *Catal. Today*, 2020, **339**, 337–343.
- J. Ye, L. Gagliardi, C. J. Cramer and D. G. Truhlar, *J. Catal.*, 2018, **360**, 160–167.
- Y.-Y. Cao, X.-F. Guo and H. Wang, *Sens. Actuators, B*, 2017, **243**, 8–13.
- K. J. Hartlieb, D. P. Ferris, J. M. Holcroft, I. Kandela, C. L. Stern, M. S. Nassar, Y. Y. Botros and J. F. Stoddart, *Mol. Pharm.*, 2017, **14**, 1831–1839.
- H. Li, N. Lv, X. Li, B. Liu, J. Feng, X. Ren, T. Guo, D. Chen, J. F. Stoddart, R. Gref and J. Zhang, *Nanoscale*, 2017, **9**, 7454–7463.
- J. Liu, T.-Y. Bao, X.-Y. Yang, P.-P. Zhu, L.-H. Wu, J.-Q. Sha, L. Zhang, L.-Z. Dong, X.-L. Cao and Y.-Q. Lan, *Chem. Commun.*, 2017, **53**, 7804–7807.
- R. A. Smaldone, R. S. Forgan, H. Furukawa, J. J. Gassensmith, A. M. Z. Slawin, O. M. Yaghi and J. F. Stoddart, *Angew. Chem., Int. Ed.*, 2010, **49**, 8630–8634.
- R. S. Forgan, R. A. Smaldone, J. J. Gassensmith, H. Furukawa, D. B. Cordes, Q. Li, C. E. Wilmer, Y. Y. Botros, R. Q. Snurr, A. M. Z. Slawin and J. F. Stoddart, *J. Am. Chem. Soc.*, 2012, **134**, 406–417.
- B. Liu, H. Li, X. Xu, X. Li, N. Lv, V. Singh, J. F. Stoddart, P. York, X. Xu, R. Gref and J. Zhang, *Int. J. Pharm.*, 2016, **514**, 212–219.
- Y. He, W. Zhang, T. Guo, G. Zhang, W. Qin, L. Zhang, C. Wang, W. Zhu, M. Yang, X. Hu, V. Singh, L. Wu, R. Gref and J. Zhang, *Acta Pharm. Sin. B*, 2019, **9**, 97–106.
- V. Singh, T. Guo, H. Xu, L. Wu, J. Gu, C. Wu, R. Gref and J. Zhang, *Chem. Commun.*, 2017, **53**, 9246–9249.
- W. Zhang, T. Guo, C. Wang, Y. He, X. Zhang, G. Li, Y. Chen, J. Li, Y. Lin, X. Xu, L. Wu, S. Zhang and J. Zhang, *Pharm. Res.*, 2019, **36**, 117.
- H. Li, J. Zhu, C. Wang, W. Qin, X. Hu, J. Tong, L. Yu, G. Zhang, X. Ren, Z. Li and J. Zhang, *Int. J. Pharm.*, 2020, **587**, 119649.
- Y. Liu, P. Zhou, Z. Cao, W. Liang, J. Yan, H. Xu, L. Wu, L. Sun, L. Gong, C. Peng, T. Guo, C. Wang and J. Zhang, *Int. J. Pharm.*, 2022, **619**, 121685.
- S.-R. Li, F.-D. Ren, L. Wang and Y.-Z. Chen, *RSC Adv.*, 2021, **11**, 35326–35330.
- W. Xiang, S. Gebhardt, R. Gläser and C.-j. Liu, *Microporous Mesoporous Mater.*, 2020, **300**, 110152.
- B. Rungtaweeworanit, J. Baek, J. R. Araujo, B. S. Archanjo, K. M. Choi, O. M. Yaghi and G. A. Somorjai, *Nano Lett.*, 2016, **16**, 7645–7649.
- X.-H. Liu, J.-G. Ma, Z. Niu, G.-M. Yang and P. Cheng, *Angew. Chem., Int. Ed.*, 2015, **54**, 988–991.





- 25 D. Jiang, G. Fang, Y. Tong, X. Wu, Y. Wang, D. Hong, W. Leng, Z. Liang, P. Tu, L. Liu, K. Xu, J. Ni and X. Li, *ACS Catal.*, 2018, **8**, 11973–11978.
- 26 D. Shi, R. Zheng, C.-S. Liu, D.-M. Chen, J. Zhao and M. Du, *Inorg. Chem.*, 2019, **58**, 7229–7235.
- 27 V. Jabbari, J. M. Veleta, M. Zarei-Chaleshtori, J. Gardea-Torresdey and D. Villagrán, *Chem. Eng. J.*, 2016, **304**, 774–783.
- 28 J. Aguilera-Sigalat and D. Bradshaw, *Coord. Chem. Rev.*, 2016, **307**, 267–291.
- 29 S. Chen, Y. Xu and M. C. Qian, *J. Agric. Food Chem.*, 2013, **61**, 11295–11302.
- 30 D. Wu, J. Cheng, T. Wang, P. Liu, L. Yang and D. Jia, *ACS Sustainable Chem. Eng.*, 2019, **7**, 12138–12147.
- 31 C.-H. Kuo, C.-J. Shieh, S.-M. Huang, H.-M. David Wang and C.-Y. Huang, *Food Hydrocolloids*, 2019, **94**, 363–370.
- 32 C. Qiu, D. J. McClements, Z. Jin, C. Wang, Y. Qin, X. Xu and J. Wang, *J. Colloid Interface Sci.*, 2019, **553**, 549–556.
- 33 Y. Chen, B. Yu, Y. Cui, S. Xu and J. Gong, *Chem. Mater.*, 2019, **31**, 1289–1295.
- 34 M. P. Abuçafy, B. L. Caetano, B. G. Chiari-Andréo, B. Fonseca-Santos, A. M. do Santos, M. Chorilli and L. A. Chiavacci, *Eur. J. Pharm. Biopharm.*, 2018, **127**, 112–119.
- 35 B. Liu, Y. He, L. Han, V. Singh, X. Xu, T. Guo, F. Meng, X. Xu, P. York, Z. Liu and J. Zhang, *Cryst. Growth Des.*, 2017, **17**, 1654–1660.
- 36 Y. Furukawa, T. Ishiwata, K. Sugikawa, K. Kokado and K. Sada, *Angew. Chem., Int. Ed.*, 2012, **51**, 10566–10569.
- 37 H. Li, M. R. Hill, R. Huang, C. Doblin, S. Lim, A. J. Hill, R. Babarao and P. Falcaro, *Chem. Commun.*, 2016, **52**, 5973–5976.
- 38 M. Y. Piao, H. J. Kim, J. K. Seo, T. S. Park, J. S. Yoon, K. H. Kim and J. K. Ha, *Asian-Australas. J. Anim. Sci.*, 2012, **25**, 1568–1574.
- 39 C.-D. Jeong, L. L. Mamuad, J. Y. Ko, H. G. Sung, K. K. Park, Y. K. Lee and S.-S. Lee, *J. Anim. Sci. Technol.*, 2016, **58**, 4.
- 40 R. V. Manaois and A. V. Morales, *J. Food Qual.*, 2014, **37**, 196–202.
- 41 N. Nagai, N. Shindo, A. Wada, H. Izu, T. Fujii, K. Matsubara, Y. Wada and N. Sakane, *J. Prev. Alzheimers Dis.*, 2020, **7**, 95–103.
- 42 S. Wang, X. Yang, W. Lu, N. Jiang, G. Zhang, Z. Cheng and W. Liu, *J. Drug Delivery Sci. Technol.*, 2021, **64**, 102593.

